Defect Assessment of Brazed Steel Components

The defect tolerance of brazed martensitic stainless steel joints subject to static or cycling loading was investigated

BY C. LEINENBACH, M. KOSTER, A. LIS, AND H. J. SCHINDLER

C. LEINENBACH (christian.leinenbach@empa.ch), *M. KOSTER, and A. LIS are with Empa-Swiss Federal Laboratories for Materials Science and Technology, Laboratory of Joining Technologies and Corrosion, Dübendorf, Switzerland. H. J. SCHINDLER is with Mat-Tec AG, Winterthur, Switzerland.*

This presentation was selected as the best brazing paper at the 5th International Brazing and Soldering Conference, April 22–25, Las Vegas, Nev.

Introduction

Brazed components play an essential role in consistent joining techniques. The brazing process is characterized by low process temperatures and fast processing times, compared to welding techniques. Beside the resulting low manufacturing costs, brazing can join dissimilar materials, e.g. metals and ceramics. Consequently, brazing provides potential for many industrial applications like the production of power electronic devices, in automotive engineering, and for power generation. Simultaneously, brazing provides potentials for seminal applications, such as for the production of structures for particle accelerators and in space technology, as well as for heat exchanging systems for hydrogen energy production.

With the use of advanced furnace brazing methods (Ref.1), brazing of steel structures becomes more economical and efficient. High-temperature (HT) furnace brazing is performed at temperatures > 900°C in vacuum or with a shielding gas. These brazed components (e.g., compressor impellers or turbine parts) are subjected to complex loading conditions in service, comprising mechanical, thermal, or thermomechanical loads (Ref. 2).

Brazed joints form a heterogeneous anisotropic system consisting of the base metals, the diffusion zone, and the filler metal. Under mechanical loading, the properties of the system vary significantly from those of the individual joining partners. The different elastic-plastic properties of the filler metal and the base metal lead to a triaxial stress state in the brazing zone, caused by constraining effects of the base metal on the filler metal alloy. As a result, large hydrostatic stresses occur in the braze layer and the ultimate tensile strength of the joint can be several times higher than the strength of the unconstrained layer material (Refs. 3, 4). Furthermore, defects such as pores or incomplete joint filling may arise during brazing and act as stress concentration sites, leading to crack initiation, propagation, and spontaneous failure. Consequently, it is very important to estimate the influence of defects on the quasistatic properties and on the fatigue behavior of brazed components. To estimate the influence of defects on bulk materials and on welded structures, defect assess-

Table 1 — Chemical Composition AISI CA 6-NM (wt %)

	C	Si	Mn	Cr	Mo	P	Ni
Min.	—	—	—	12	0.3	—	3.5
Max.	0.05	0.70	1.50	14	0.7	0.04	4.5

Table 2 — Mechanical Properties of AISI CA 6-NM

E (MPa)	σ_y (MPa)	σ_{UTS} (MPa)	A (%)
203500	1017	1224	16.7

ment procedures, such as R6, BS7910, or SINTAP, have been developed for quasi-static loading conditions (Refs. 5–7). Considering the defect assessment of brazed components, little information is available (Ref. 8). Almost no information can be found regarding the behavior of braze joints under cyclic loading (Ref. 9). Preliminary investigations on the fatigue crack propagation in brazing show that the joints are characterized by an unusually high Paris exponent between 11 and 13 (Refs. 10, 11).

In the present work, the applicability of defect assessment procedures on brazed joints was investigated by combining experimental techniques and theoretical models. Furthermore, a method was established to estimate the influence of different defects on low-cycle fatigue (LCF) behavior.

Testing Materials and Experimental Setup

The brazed joints used for the following investigations consisted of the soft martensitic stainless steel X3CrNiMo13-4 (AISI CA 6-NM) as base metal. The chemical composition of the steel is shown in Table 1.

The steel's martensitic-ferritic microstructure provides high strength and high elongation to fracture, according to Table 2. Its excellent mechanical properties and corrosion behavior as well as its thermal resistance qualify the steel for the production of highly loaded pumps, compressors, or water turbines. Steel plates with the dimensions 300 × 100 × 25 mm were brazed, using foils of the binary alloy Au-18Ni ($T_m \approx 955°C$) with a thickness of 100 μm as filler metal. Brazing was performed with a special brazing jig in an industrial shielding gas furnace (SOLO Profitherm 600) at a temperature of 1020°C for 20 min. After cooling down to room temperature, the specimens were tempered at 520°C for 5.5 h in nitrogen atmosphere.

Beside standard round tensile specimens according to DIN 50125, round fatigue specimens with gauge length diameters of 4 and 5 mm were used for the experiments — Fig. 1A. To determine the geometry effect on the joint strength, special T-joint geometry specimens (Fig. 1B) were manufactured. The T-joint geometry is often realized in technical components. The specimens are characterized by an abrupt change of the cross section and, consequently, by the highest loads occurring in the braze layer. The T-joint geometry was also used to study the influence of brazing defects on the mechanical properties. Artificial defects with different geometries (straight and semielliptical) were introduced into the brazing zone by electrical discharge machining (EDM), using a wire with a diameter of 0.3 mm for the straight defects and a shaped Cu plate for the semielliptical defects (Fig. 2). To investigate the influence of the defect size, specimens containing straight defects with a size of a = 0.5 mm, a = 1 mm, and a = 2 mm were investigated. For the semielliptical defects, a = 0.75 mm, a = 1.5 mm, and a = 3 mm, with a ratio of a/c = 2/3 were selected.

Tensile tests were performed on an electromechanical testing machine (Schenck Trebel RSA 250 kN) after DIN EN 10002. For the fatigue experiments, a servo-hydraulic testing facility was used (Schenk Hydroplus 5666). The fatigue experiments were performed in the LCF regime until a maximum number of loading cycles of $N_{max} = 2 \cdot 10^4$ was reached to simulate the influence of start/stop cycles on highly loaded brazed compressor impellers. The tests were performed at a load ratio of R = 0.1 with a sinusoidal load at a frequency of 1 Hz.

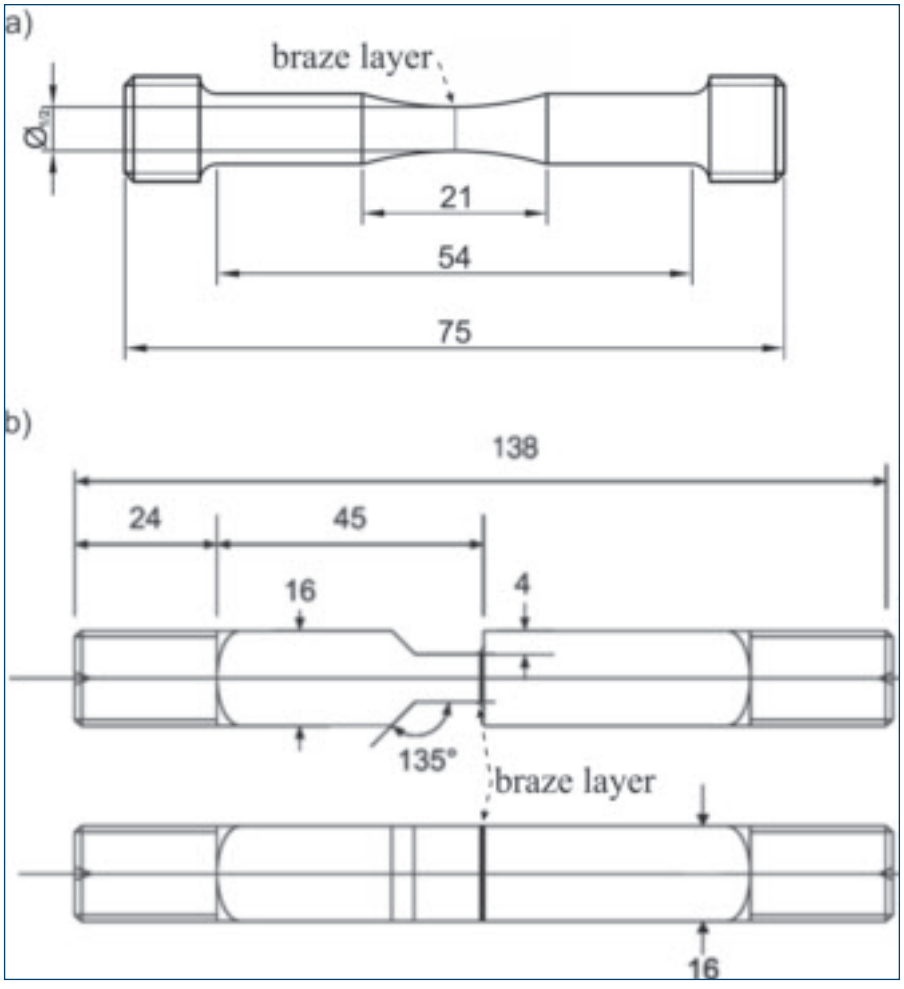

Fig. 1 — A — Standard round specimen; B — T-joint specimen geometry.

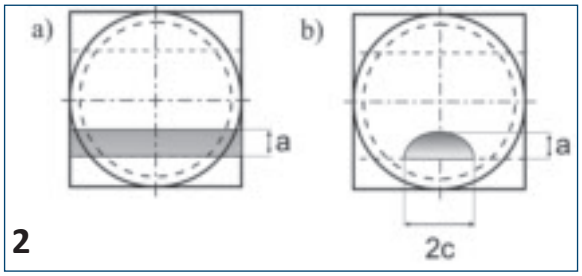

Fig. 2 — Schematics of defects. A —Straight; B — semielliptical.

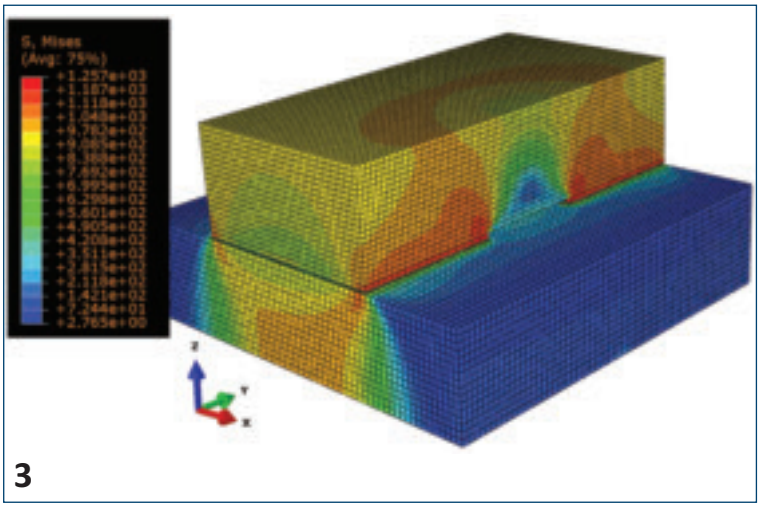

Fig. 3 — Von Mises stress distribution in a T-joint with semielliptical defect.

Finite Element Simulations

The tensile tests with T-joint specimens were additionally simulated by FE methods. The aim was to numerically determine the critical limit loads. A 3-D model of the complex joint geometries was created with the FE software Abaqus 6.10-EF. Ideal metallic bonding between the steel and the filler metal was assumed. A mesh of hexahedral brick elements with 8 nodes (C3D8R) was created. In the brazing zone, the element size was set to 0.05 mm, whereas the element size in the base material was set to 0.25 mm. The mesh size was chosen as an optimum between the accuracy of the simulated load-displacement result and the FE solution time. The deformation behavior was described by an elastic-plastic deformation law based on Ramberg-Osgood according to Equation 1.

$$\varepsilon = \frac{\sigma}{E} + \alpha \cdot \frac{\sigma}{E} \cdot \frac{\sigma^{n-1}}{\sigma_y} \quad (1)$$

The material parameters were derived from the stress-strain curves determined as described in Ref. 2 and from Table 2. The structure in Fig. 3 was loaded on the upper surface with a homogeneous tensile stress distribution, whereas the bottom surface was fixed by the boundary condition $u_z = 0$. The specimen was defined to fail when the plastic strain at the interface between base metal and filler metal exceeded a critical value of $\varepsilon_{pl,crit} = 0.015$, which means when the base material becomes fully plastic. In Fig. 3, the meshed specimen and the resulting von Mises stress distribution of a specimen with a semielliptical defect subjected to tensile loading at the critical external stress is presented. As expected, high stress concentrations are located around the defect, which even affect the base metal in a widely spread volume.

Defect Assessment for Static Loading

Tensile tests were performed to estimate the influence of different specimen geometries and of different defects on the quasistatic joint strength. In a first series of experiments, standard round specimens were tested. The results served as a reference for further experiments. The ultimate tensile strength (σ_{UTS}) of standard round specimens averages 1084 MPa. Experiments with T-joint specimens show that the change of the specimen geometry leads to an increase of σ_{UTS} to 1120 MPa (Table 3).

The increase of σ_{UTS} can be explained by the T-joint geometry, which leads to a triaxial stress state at the change of the cross section. The multiaxial stress state leads to constraining effects on the ductile filler metal. Consequently, the deformation in the braze layer is restricted, which leads to a decrease of the effective stresses under quasistatic loading conditions. Further tensile tests were performed to study the influence of the different defects on the quasistatic joint strength. As expected, defect-containing specimens showed considerably lower ultimate tensile strengths than the defect-free reference specimens. The decrease of the tensile strength is closely related to the size and shape of the defect introduced in the braze layer. The lowest ulti-

Table 3 — Experimental Results of the Tensile Tests and Fatigue Experiments

Defect Type	Defect Size a (mm)	σ_{UTS} (MPa)	$\Delta\sigma_{nom,\ 20000}$ (MPa)
None, round	0	1084	800
None, T-joint	0	1120	450
Straight	0.5	—	270
	1	582	180
	2	450	135
Semielliptical	0.75	—	360
	1.5	936	282
	3	674	270

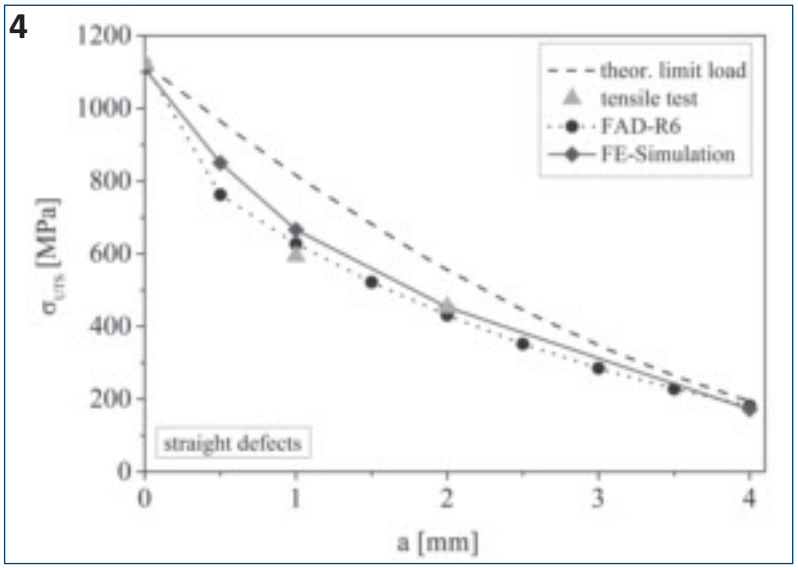

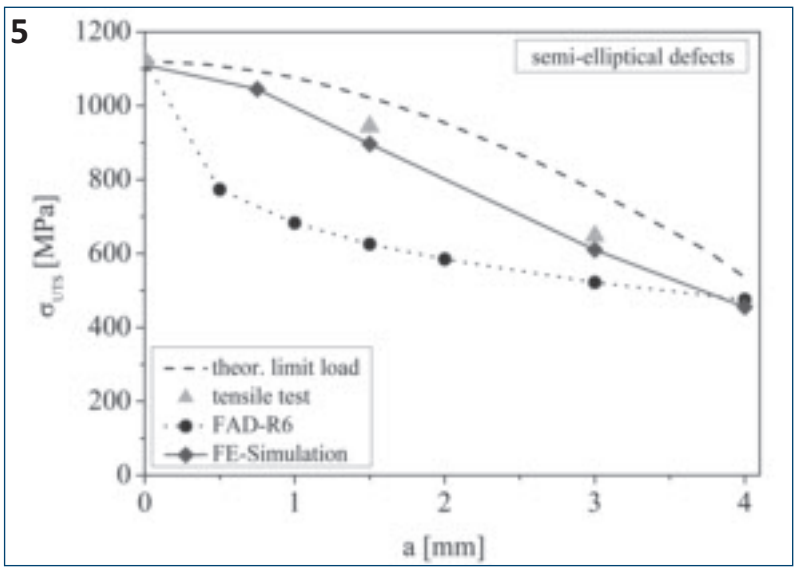

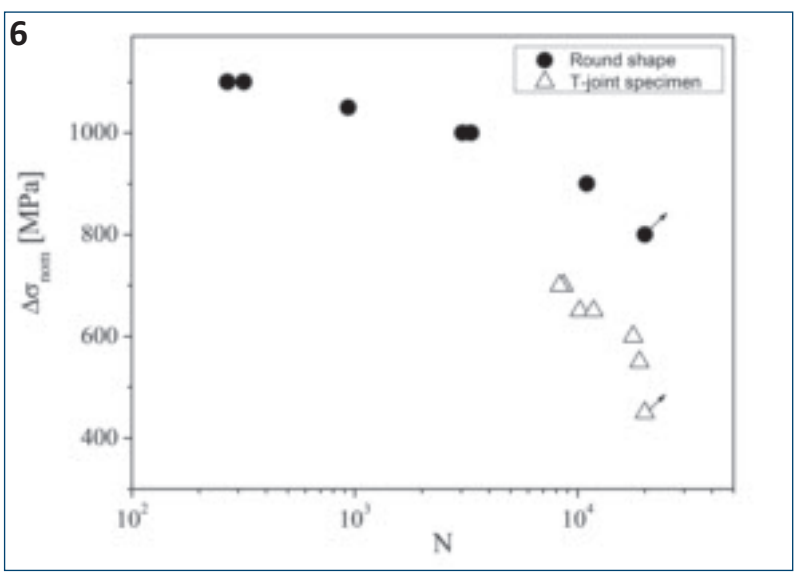

Fig. 4 — Influence of straight defects on s_{UTS}.

Fig. 5 — Influence of semielliptical defects on s_{UTS}.

Fig. 6 — Influence of the specimen geometry on $Ds_{nom,20000}$.

mate strength of σ_{UTS} = 450 MPa was obtained for a specimen containing a straight defect with a size of a = 2 mm.

Further investigations of the defect influence on σ_{UTS} serve to compare the experimental results with the limit loads, calculated with the defect assessment procedure R6, option 3. Furthermore, the experimental results were used to verify failure criteria in the scope of FE calculations.

A comparison of the tensile tests with the defect assessment procedure for straight defects is shown in Fig. 4. The results were further compared with the theoretical limit load, which only takes into account the reduction of the cross section in the brazing zone due to the defects, but not the corresponding stress concentrations.

The highest tolerable loads determined in the scope of FE calculations and limit loads according the R6 procedure are in good agreement with the experimental results.

While for the semielliptical defects the FE calculations show a good correlation with the experimental results, the R6 procedure tends to provide conservative limit loads — Fig. 5.

The investigations of the quasistatic properties have shown that the influence of defects leads to a decrease in the ultimate tensile strengths. Furthermore, it could be shown that the R6 method is generally applicable for the investigated T-joint specimens, but lead to a very conservative prediction of the joint strength. The performed FE calculations are the most appropriate method to evaluate the influence of defects of varying shape and size. These calculations allow to respect the specimen geometry and the individual elastic-plastic properties of the base metal and the filler metal alloy. Based on these good results, further investigations

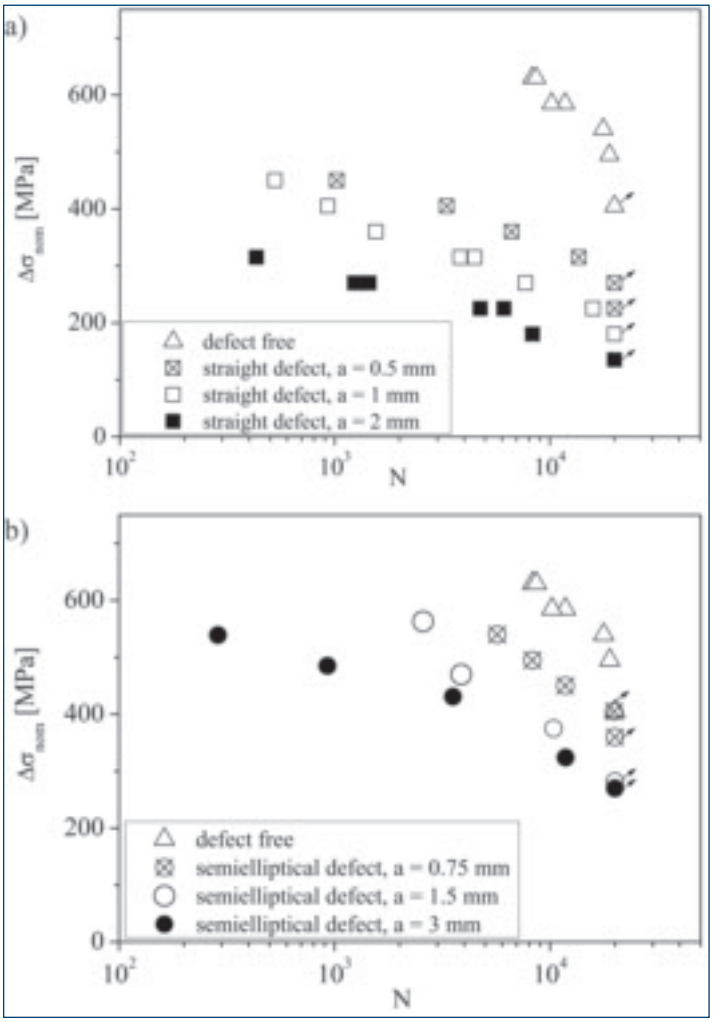

Fig. 7 — Influence on $\Delta\sigma_{nom,20000}$. A — Straight defects; B — semielliptical defects.

will be performed about the transferability of the developed method on different steel heat treatments.

Defect Assessment for Cyclic Loading

To investigate the influence of the specimen geometry and of defects on the LCF fatigue behavior, cyclic loading experiments were performed. In relation to the tensile tests, round-shaped specimens, as well as T-joint specimens, were tested. The influence of defects was quantified for T-joint specimens. The maximum tolerable stress range $\Delta\sigma_{nom,20000}$ to reach N_{max} failure free of the round-shaped specimen serves as reference for the T-joint specimens.

The results of the fatigue experiments show that the specimen geometry has a significant influence on $\Delta\sigma_{nom,20000}$ (Fig. 6 and Table 3). While for standard round-shaped specimens $\Delta\sigma_{nom,20000}$ is 800 MPa, the change of the specimen geometry leads to a decrease of $\Delta\sigma_{nom,20000}$ to 450 MPa for the defect-free T-joint specimens. Further fatigue experiments with defect-containing specimens show a pronounced influence of defect size and geometry on $\Delta\sigma_{nom,20000}$.

Figure 7A shows the resulting S,N curves for specimens containing straight defects with different sizes. The S,N-curves for specimens containing semielliptical defects are shown in Fig. 7B. In the two diagrams, the defect-free T-joint specimens were considered as a reference.

As expected, the defect- containing specimens provide significantly lower $\Delta\sigma_{nom,20000}$ compared to the defect-free reference specimens, and $\Delta\sigma_{nom,20000}$ decreases with increasing defect size. Furthermore, the decrease in $\Delta\sigma_{nom,20000}$ is more pronounced for straight defects compared to semielliptical defects. A straight defect with a size of a = 2 mm leads to a reduction of $\Delta\sigma_{nom,20000}$ to 135 MPa, whereas a joint with a semielliptical defect of a = 3 mm provides $\Delta\sigma_{nom,20000}$ = 270 MPa. The smallest semielliptical defect (a = 0.75 mm) exhibited the highest tolerable stress range of $\Delta\sigma_{nom,20000}$ = 360 MPa, and almost reaches $\Delta\sigma_{nom,20000}$ of the defect- free T-joint specimen.

The results show that the influence of a defined defect can be estimated with the related S,N curve, but the direct comparison of different defects (straight defects compared with semielliptical defects) is not possible. Consequently, S,N curves are not applicable to estimate the influence of real defects, because real defects vary continuously in size, shape, and position.

Generally, the influence of a defect results in a local increase in the stress concentration. According to the notch stress concept, the increase in the local stresses is closely related to the notch radius (ρ) and to the notch depth (a_n) — Fig. 8A.

The geometry of characteristic brazing defects as well as the geometry of the artificial defects considered in this work corresponds to a sharp notch. The difference between a sharp notch and a crack (Fig. 8B) subjected to cyclic loading is that for notches a certain number of loading cycles is required to initiate a fatigue crack. The initiation period decreases with decreasing notch radius. According to our previous work, it can be assumed that the crack propagation period can be neglected for the present loading cases and specimens (Refs. 10, 11).

The number of cycles required for initiating a fatigue crack is dependent on the local fatigue conditions. For sharp notches, the local stress at the notch tip,

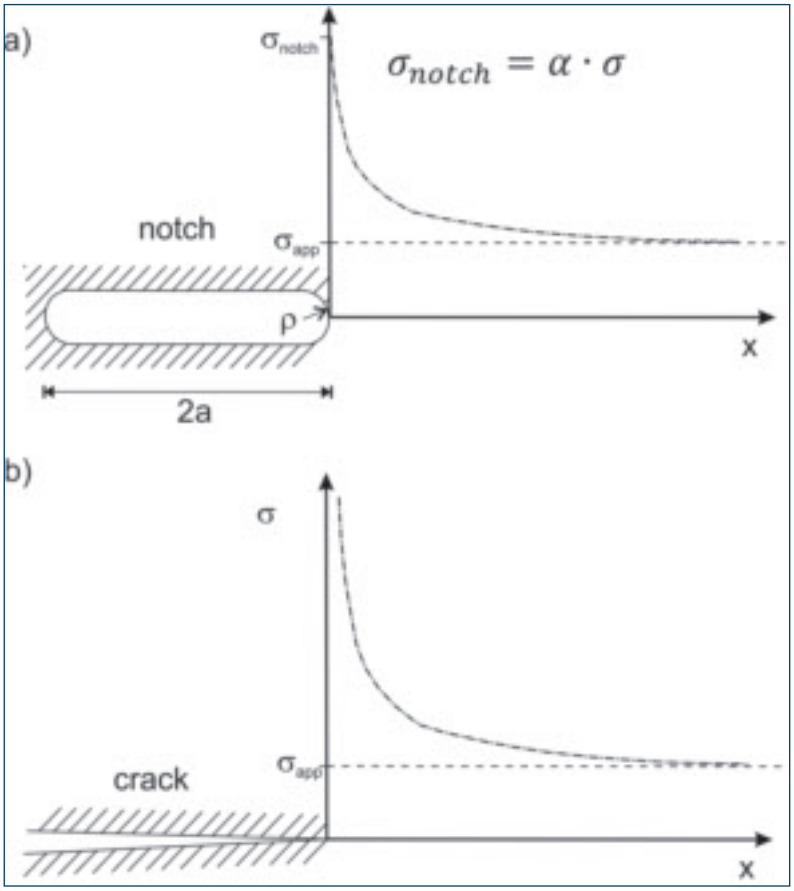

Fig. 8 — Stress distribution. A — Ahead of a notch; B — a crack.

$\sigma_{loc,max}$, is correlated with the stress intensity factor K_I, according to Equation 2.

$$K_I = \frac{\sigma_{loc,max} \cdot \sqrt{\pi\rho}}{2} \quad (2)$$

The stress intensity factor is further dependent on the specimen geometry, the defect geometry, and the nominal stress perpendicular to the defective braze layer.

Based on experimental results and FE calculations, the stress intensities have been calculated (Ref. 8). For specimens with a T-joint geometry, a dimensionless factor (k) was derived. This factor serves to calculate K_I as a function of the maximum applied load ($\sigma_{nom,max}$) and of the specimen width (W) according to Equation 3.

$$K_{I,max} = k \cdot W^{1/2} \cdot \sigma_{nom,max} \quad (3)$$

Figure 9 shows the curve of k for straight and semielliptical defects as a function of the crack length a. With increasing crack length, the rising k-values indicate increasing stress intensities. From a critical size (a > 1 mm), the rise of the k factor is more pronounced for straight defects.

With the proposed method, it is possible to calculate the stress intensities caused by a defect and plot the resulting values in a ΔK_I,N curve similar to conventional S,N curves. The resulting graph is shown in Fig. 10.

In the ΔK_I,N curve, the results for the specimens with different defect geometries and sizes fall into a relatively small band, indicating that the proposed method allows a direct comparison of different defect geometries.

Moreover, it is possible to assign notch intensity factors to defect-free T-joint specimens. The extrapolation of the k curve (Fig. 9) to a = 0 mm leads to a value of k = 0.41. Figure 10 also contains the results for the defect-free T-joints as $\Delta K_{I,N}$,N data and shows that the experimental results are in remarkably good agreement with the values for joints containing defects. This shows that macroscopic notches like the change of the cross section in a T-joint can be described by fracture mechanics approaches. It is, therefore, concluded that the fatigue behavior of defect-containing brazed specimens is only weakly influenced by the local notch geometry and that the procedure can be applied to real brazing defects.

Conclusions

The performed experiments show a significant influence of brazing defects and specimen geometry on the resulting joint strengths. Tensile tests have shown that, due to a multiaxial stress state, σ_{UTS} of T-joint specimens exceeds the ultimate tensile strength of standard round specimens. Furthermore, the influence of defects leads to a pronounced decrease of σ_{UTS}. A comparison of the experimental results shows the defect assessment procedure R6 can generally be used for the estimation of defects on the quasistatic properties. For changing defect geometries, the R6 procedure deviates from the experimental results, but gives a conservative estimation. Finite element calculations seem to be the most adequate tool to determine the influence of defects on the quasistatic properties because they respect individual materials properties and allow investigating local effects. At the same time, they serve to determine values for the estimation of a defect's influence on the fatigue behavior.

In the scope of fatigue experiments, the maximum tolerable loadings ($\Delta\sigma_{nom,20000}$) until N_{max} = 20000 cycles were determined. Round-shaped specimens served as a reference for further tests with defect-free and defect-con-

Fig. 9 — k-values for straight and semi-elliptical defects.

Fig. 10 — $K_{I,max}$-N curve for the tested T-joint specimens.

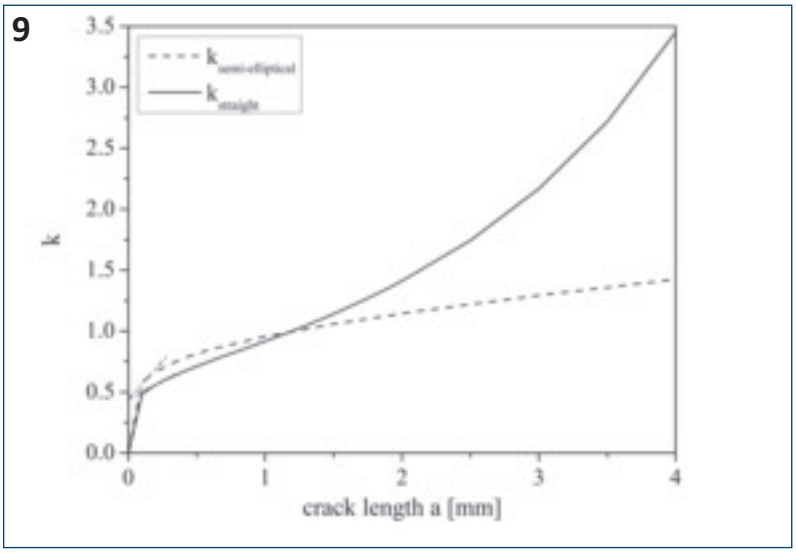

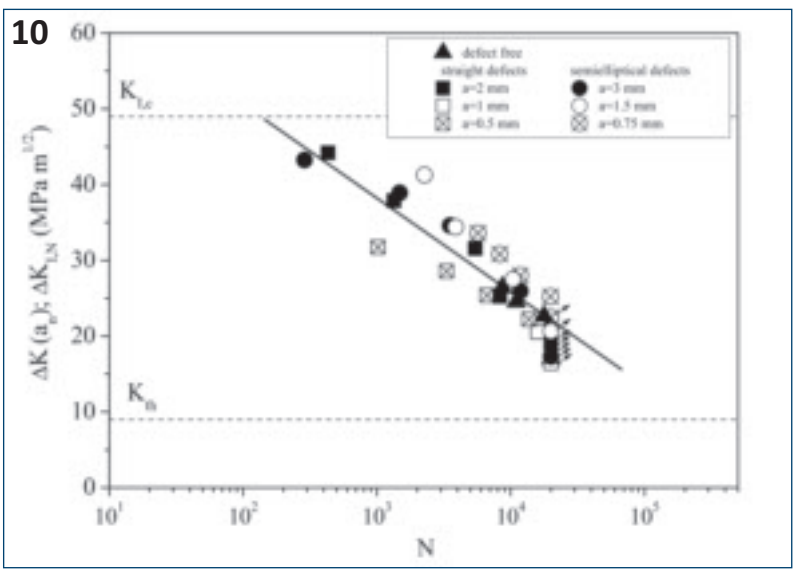

taining T-joint specimens. Considering $\Delta\sigma_{nom,20000}$, round- shaped specimens provide the highest strengths, whereas the change of the specimen geometry leads to a significant decrease of $\Delta\sigma_{nom,20000}$. The influence of defects leads to a further decrease of $\Delta\sigma_{nom,20000}$. The experiments show, that generally, $\Delta\sigma_{nom,20000}$ decreases with increasing defect size, but a direct comparison of different defect geometries is not possible with S,N curves. Due to the geometry of the introduced defect, it is possible to be considered as a sharp notch. By a combination of experimental techniques and FE calculations, it was possible to calculate the stress intensity factor K_I caused by a defect. A graph of ΔK_I over the numbers of cycles to failure shows a good correlation with the experimental results. Besides the possibility to determine the influence of different defects, the developed method also allows assigning a stress intensity factor to defect-free T-joint specimens and evaluating the fatigue behavior on a unique scale.

Acknowledgment

The authors gratefully acknowledge MAN Diesel & Turbo for the funding of this project

References

1. Feldbauer, S. L. 2004. Modern brazing of stainless steel. *Welding Journal* 83(10): 30–33.

2. Leinenbach, C., Schindler, H. J., Baser, T. A., Rüttimann, N., and Wegener, K. 2010. Quasistatic fracture behaviour and defect assessment of brazed soft martensitic stainless steel joints. *Eng. Failure Anal.* 17: 672–682.

3. Kassner, M. E., Kennedy, T. C., and Schrems, K. K. 1998. The mechanism of ductile fracture in constrained thin silver films. *Acta Mater*. 46: 6445–6457.

4. Cugnoni, J., Botsis, J., and Janczak-Rusch, J. 2006. Size and constraining effects in lead-free solder joints. *Adv. Eng. Mater*. 8: 184–191.

5. British Energy Generation, Ltd. 2002. *Assessment of the Integrity of Structures Containing Defects*. R6-Rev. 4.

6. British Standard 1999. *Guide on Methods for Assessing Acceptability of Flaws in Metallic Structures.* BS 7910.

7. Flom, Y., Wang, L., Powell, M. M. Soffa, M. A., and Rommel, M. L. 2009. Evaluating margins of safety in brazed joints. *Welding Journal* 88(10): 31–37.

8. Leinenbach, C., Lehmann, H., and Schindler, H. J. 2007. Mechanisches Verhalten und Fehlerempfindlichkeit von Hartlötverbindungen (Mechanical properties and defect sensitivity of high-temperature brazings). *MP-Materials Testing* 49: 2–9.

9. Leinenbach, C., Koster, M., and Schindler, H. J. 2012. Fatigue assessment of defect-free and defect-containing brazed steel joints. *J. Mater. Eng. Perform*., 21: 739–747.

10. Baser, T. A., Leinenbach, C., and Schindler, H. J. 2010. Fracture behavior of brazed soft martensitic stainless steel joints under cyclic loading. *Mater. Sci. Forum* 636-637: 1490–1495.

11. Schindler H. J., and Leinenbach C. 2012. Mechanics of fatigue crack growth in a bonding interface. *Eng. Fract. Mech.,* accepted, DOI: 10.1016/j.engfracmech.2012.04.009.